

A self-powered and concealed sensor based on triboelectric nanogenerators for cultural-relic anti-theft systems

Baocheng wang^{1,2}, Xiaoying Zhai³, Xuelian Wei^{1,2}, Yapeng Shi^{1,2}, Xiaoqing Huo^{1,2}, Ruonan Li¹, Zhiyi Wu^{1,2,4} (✉), and Zhong Lin Wang^{1,2,4,5} (✉)

¹ Beijing Institute of Nanoenergy and Nanosystems, Chinese Academy of Sciences, Beijing 101400, China

² College of Nanoscience and Technology, University of Chinese Academy of Science, Beijing 100049, China

³ Queen Mary University of London Engineering School, Northwestern Polytechnical University, Xi'an 710072, China

⁴ CUSTech Institute of Technology, Wenzhou 325024, China

⁵ School of Materials Science and Engineering, Georgia Institute of Technology, Atlanta, GA 30332, USA

© Tsinghua University Press 2022

Received: 18 February 2022 / Revised: 16 April 2022 / Accepted: 19 April 2022

ABSTRACT

The theft prevention for cultural relics in museums, field excavation sites, and temporary exhibition events is of extreme importance. However, traditional anti-theft technologies such as infrared monitoring and radio frequency identification are highly costly, power-consuming, and easy to break. Here, a transparent, ultrathin, and flexible triboelectric sensor (TUFS) with a simple and low-cost method is proposed. With a thickness, weight, and transmittance of 92 μm , 0.12 g, and 89.4%, the TUFS manifests superb concealment. Benefiting from the characteristic of triboelectric nanogenerators, the TUFS responds effectively to common cultural-relic materials. Moreover, distinguished electrical responses can be obtained even for very small weights (10 g) and areas (1 cm^2), proving the sensitivity and wide range of use of the TUFS. Finally, we construct a concealed cultural-relic anti-theft system that enables real-time alarming and accurate positioning of cultural relics, which is expected to strengthen the security level of the existing museum anti-theft systems.

KEYWORDS

concealed sensor, self-powered, triboelectric nanogenerator, cultural relic, anti-theft

1 Introduction

China is an ancient civilization with a history dating back over 5,000 years. A large number of cultural treasures have been discovered whose value is enormous. However, more and more cultural treasures have been stolen by criminals, resulting in uncountable losses. Therefore, effective anti-theft systems for cultural relics are of extreme importance. Currently, camera-based systems (with infrared detectors) are commonly adopted in artifacts anti-theft [1, 2]. However, such systems are susceptible to thermostats such as air conditioners. Moreover, this system will not work effectively if the probe of the infrared detector is obscured by criminals. Radio frequency identification (RFID) has recently been applied in the cultural-relic anti-theft system [3, 4]. If the cultural relic with an electronic tag leaves the effective identification range, the system will sound an alarm immediately. However, the RFID system has a limited recognition range, and the barrier between the reader and the tag can affect the signal strength. Additionally, the implementation and operation of these systems are highly costly and power-consuming. It can be concluded that the above anti-theft systems all have limitations and need another anti-theft technology to strengthen their security level.

It is a possible solution to place sensors on interfaces between cultural relics and exhibition stands or walls. The commonly

adopted sensors are based on piezoelectric, capacitive, resistive, and triboelectric mechanism [5–8]. Particularly, triboelectric nanogenerators (TENGs) can directly convert the detected information into electric signals, which use Maxwell's displacement current as the internal driving force [9–11]. Based on the coupling of contact electrification and electrostatic induction, TENGs have a series of advantages of lightweight, flexibility, low cost, and diversity of material selection [12–17]. Hence TENGs are widely applied in both energy supply and self-powered sensing [18–33]. It is undeniable that TENG is an ideal technology for cultural relics monitoring. Ke et al. proposed a high-performance Al/polydimethylsiloxane (PDMS)-TENG with a complex morphology of overlapped deep two-height microneedles, highlighting its superb pressure sensitivity [34]. Nonetheless, its structure, double electrodes with a cavity, is not suitable for monitoring artifacts. Once the artifact is moved after being positioned in one place for a long time, the double-electrode structure may not separate effectively. Consequently, a single-electrode structure TENG is more suitable. Shi et al. developed a flexible TENG by sandwiching a silver nanowire electrode between a thermoplastic polyurethane sensing layer and a poly(vinylalcohol)/chitosan substrate [35]. The electrospinning polyurethane sensing layer demonstrates a high output, whereas the transparency is not good, which is not suitable to construct a concealed cultural-relic anti-theft system. Therefore, low-cost, easy-

to-fabricate, highly sensitive, and good-concealment triboelectric sensors are highly desired for constructing cultural-relic anti-theft systems.

Here, we fabricated a transparent, ultrathin, and flexible triboelectric sensor (TUFs) with a simple and low-cost method (coating PDMS uniformly on an indium tin oxide-polyethylene terephthalate (ITO-PET) substrate). Through rationally selecting materials and adjusting the spin coating parameters, TUFs's thickness, weight, and transmittance are 92 μm , 0.12 g, and 89.4%, respectively, manifesting superb concealment. Besides, the TUFs responds effectively to rice paper, wood, iron, porcelain, copper, and silk. Moreover, a 3 cm \times 3 cm TUFs can generate voltages of 0.5 and 1.5 V, when the weight is 10 g and the contact area is 1 cm \times 1 cm, respectively. Keeping contact with a weight from 1 to 30 days, the TUFs exhibits an outstanding static stability with a negligible voltage drop. And a negligible voltage drop is observed even after operating for 5,000 cycles, substantiating superior dynamic stability. Furthermore, the TUFs responds effectively toward a wine bronze cup, a pottery bottle, and a Chinese landscape painting. Moreover, the triboelectric effect is widely existing in materials, thus the TUFs is expected to be applied to a wide range of cultural relics. Finally, based on a 2 \times 2 sensor array, we built a concealed cultural-relic theft-prevention system that enables real-time alarms and accurate positioning, which is expected to strengthen the security level of the existing museum

anti-theft systems and act as the last line of protecting cultural relics from theft.

2 Results and discussion

2.1 Structure and working principle of TUFs

A potential application scenario of the cultural-relic anti-theft system is illustrated in Fig. 1(a), where TUFs are attached to surfaces of cabinets, just below cultural relics. Once a theft breaks into the museum and picks up a cultural relic, the anti-theft system will issue an alarm and determine the position of the stolen cultural relic based on the abnormal voltage signal received. Under the era of internet of things (IoT), the cultural-relic anti-theft system equipped with concealed TUFs, reveals its potential for the anti-theft of cultural relics. As shown in the enlarged diagram of Fig. 1(a), the TUFs consists of three layers: PDMS, ITO, and PET, serving as the triboelectric layer, the electrode layer, and the substrate layer, respectively. PDMS was selected as the triboelectric layer owing to its strong affinity to electrons, superior mechanical properties, and good transparency.

As described in Fig. 1(b) and Fig. S1 in the Electronic Supplementary Material (ESM), the total thickness and weight of the TUFs were 92 μm and 0.12 g respectively, presenting an ultrathin thickness and light weight. The inset shows the flexibility

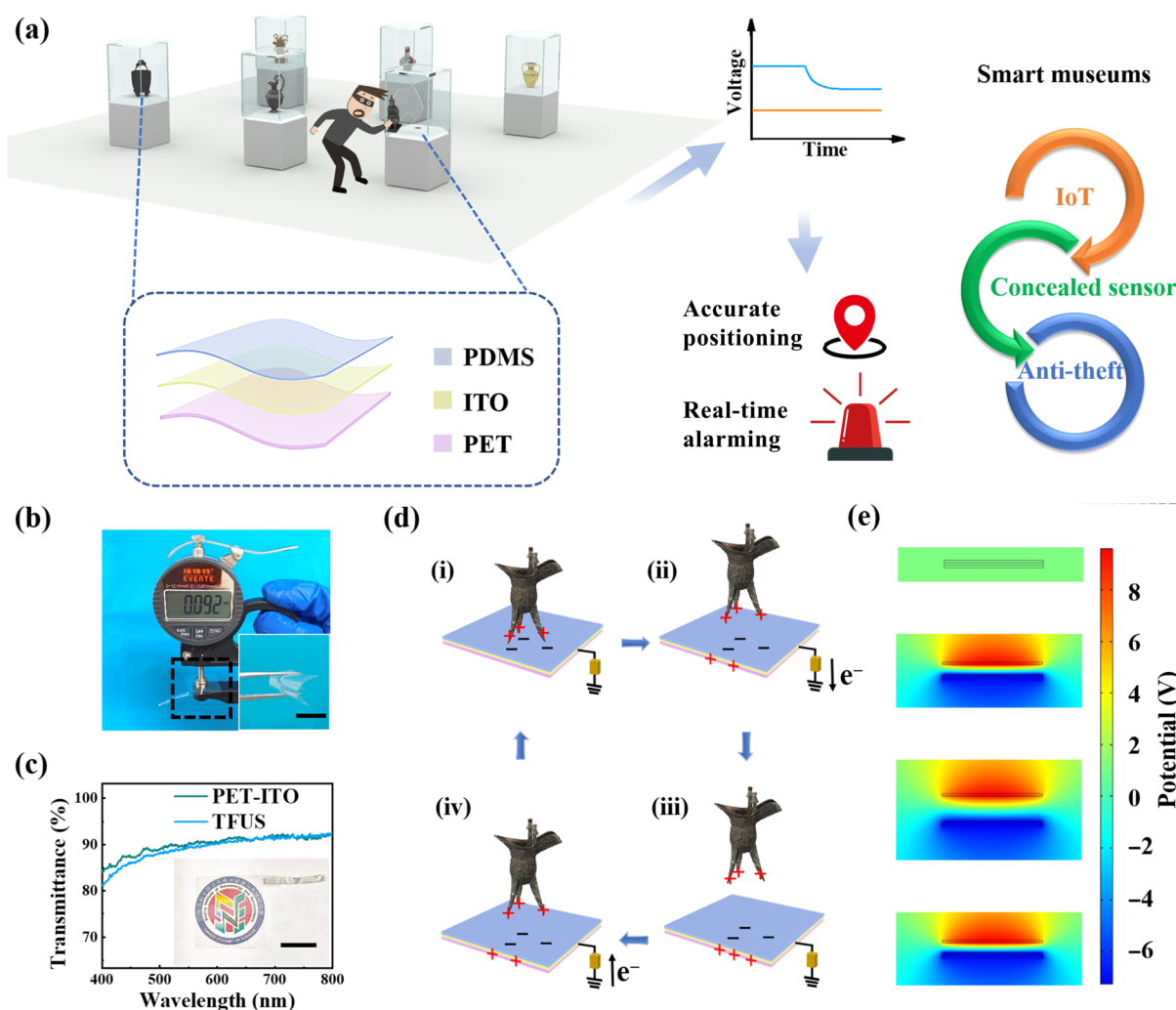


Figure 1 Structure design of the TUFs. (a) Potential application scenario of the cultural-relic anti-theft system. (b) Photograph image of the TUFs with a total thickness of 92 μm (scale bar, 2 cm). The inset shows that it can be bent easily. (c) Transmittance of the PET-ITO film and the TUFs in the visible range. The inset indicates that the TUFs is transparent to an institute badge (scale bar, 1.5 cm). (d) Working mechanisms of the single-electrode TUFs. (e) Finite element simulation of the potential distribution of the TUFs.

of the TUFs. Moreover, the sensor's transmittance is crucial, endorsing the sensor with outstanding concealment. As depicted in Fig. 1(c), a 50 μm -thick PET-ITO film shows transmittance of 90.0% in the visible light wavelength range (400–800 nm), and the TUFs shows transmittance of 89.4%, manifesting superior transparency.

In order to explore how the TUFs works so that it can be preferably applied to actual scenario, the work mechanism of the TUFs was clarified in Fig. 1(d), based on the coupling of contact electrification and electrostatic induction. When the wine vessel is in full contact with the TUFs, positive charges appear on the vessel's surface while an equal number of negative charges appear on the surface of the TUFs, owing to that affinity to electrons of PDMS is stronger than that of the vessel. The electric potential is zero between ITO and the grounding terminal, thus there are no electrons flowing in the external circuit (Fig. 1(d)-(i)). As the vessel is separating from the TUFs's surface, a negative electric potential is generated between ITO and the grounding terminal, driving electrons flowing from the external circuit (Fig. 1(d)-(ii)). When the vessel is fully separated from the TUFs, the transferred charges on ITO generate a positive electric potential, which offsets the negative electric potential. Consequently, electric potential is balanced again and there is no electric current in the external circuit (Fig. 1(d)-(iii)). When the vessel is approaching the TUFs's surface, the electric potential balance is broken. A positive electric potential drives the electrons flowing from the grounding terminal to ITO (Fig. 1(d)-(iv)). Consequently, an alternating voltage is

generated. As shown in Fig. 1(e), the corresponding electric potential is simulated by COMSOL.

2.2 Electrical characterizations for the TUFs

The detailed fabrication process of the TUFs is illustrated in Fig. 2(a). A piece of a flexible and clean ITO-coated PET film was applied as the substrate for supporting the PDMS structure. The pre-mixed liquid PDMS elastomer and curing agent were mixed, degassed, and uniformly spin-coated on the insulation surface of the substrate. After curing thermally, a uniform PDMS layer was fixed on the surface of the PET substrate. Furthermore, the water contact angle of PDMS is 106.57° , providing the TUFs with good hydrophobicity (Fig. 2(b)).

In order to investigate the fundamental electrical output performance of the TUFs, we used a linear motor to provide periodic contact-separation motions. The contact area was chosen as $3\text{ cm} \times 3\text{ cm}$ (all the electrical outputs in this paper were measured by TUFs of $3\text{ cm} \times 3\text{ cm}$), the tapping force was applied as 5 N, and the maximum movement distance was set as 10 mm. A piece of copper film was adopted as the other triboelectric layer to have a contact-separation process with the TUFs. The open-circuit voltage (V_{OC}), short-circuit current (I_{SC}), and short-circuit transferred charges (Q_{SC}) are indicated in Figs. 2(c)–2(e) with frequency from 0.5, 1, 2 to 3 Hz. As the frequency rises, the V_{OC} and Q_{SC} remain essentially constant while the I_{SC} gradually increases, which can be attributed to that V_{OC} and Q_{SC} are independent of speed. Choosing an appropriate triboelectric layer

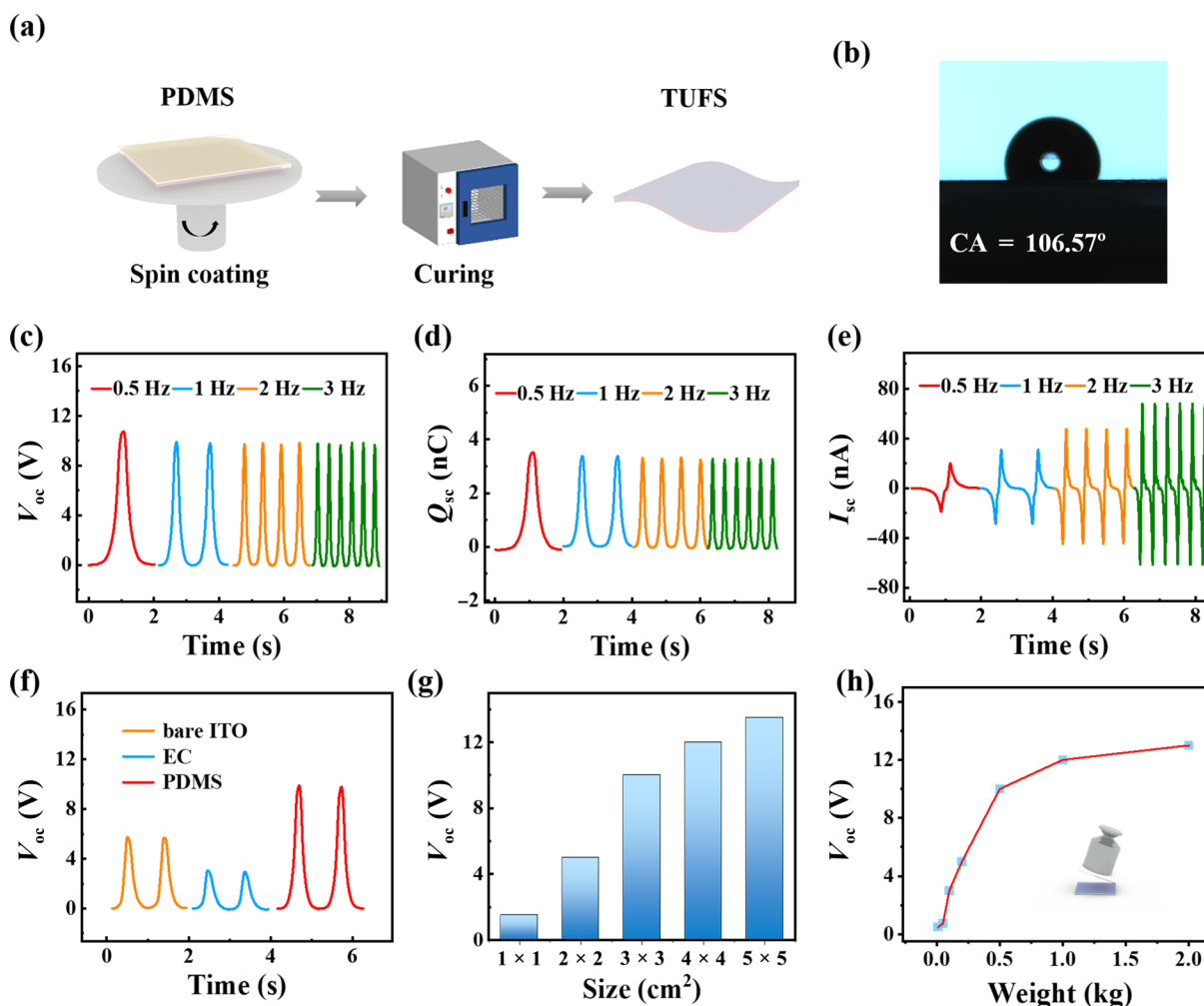


Figure 2 Fundamental electrical output performance of the TUFs. (a) Fabrication process of the TUFs. (b) Photograph of the contact angle between the PDMS and water. (c)–(e) Frequency-response characteristics (5 N). (f) V_{OC} of the bare-ITO based sensor, the EC-Based sensor, and the TUFs (5 N). (g) V_{OC} for copper films with different area (5 N). (h) V_{OC} for copper films at different weights. The inset shows the measuring scene.

is of utmost significance for the performance of the TUFs and should consider two aspects: (1) The triboelectric layer should have good transmittance in order to obtain a transparent TUFs; (2) the triboelectric layer can endow the TUFs with high output, which can enhance the sensitivity of the TUFs. PDMS and ethyl cellulose (EC) films both have good transmittance, and they both can be coated uniformly on the surface of PET-ITO film with easy fabrication methods [36]. As shown in Fig. 2(f), the order of V_{OC} from largest to smallest is as follows: the PDMS-based TUFs, the bare-ITO-based TUFs, and the EC-based TUFs. Compared with ITO and copper, PDMS and copper are farther apart on the triboelectric series [37], thus creating more charges when rubbed together in contrast with ITO and copper. As a consequence of the adhesion between EC and ITO is too weak, the induction of charges is compromised on the surface of ITO, resulting in the poor output of the EC-based TUFs. Accordingly, A PDMS film was determined as the triboelectric layer. Furthermore, the TUFs can distinguish cultural relics of different areas as shown in Fig. 2(g). The V_{OC} of the TUFs was measured for different areas of copper films at a weight of 0.5 kg. The V_{OC} increases as the area increases, seeing as a larger contact area generates a larger voltage. It is noted that the TUFs can still generate a voltage of 1.5 V at 1 cm \times 1 cm, exhibiting superb area sensitivity. Additionally, it is significant for the TUFs to respond to cultural relics of different

weights. As described in Fig. 2(h), we measured the V_{OC} at different weights. The inset shows the test scenario, where a copper film was firstly pasted on a 3 cm \times 3 cm acrylic plate (1.9 g), then a weight was attached. As the weights change from 0.01 to 2 kg, the voltage rises rapidly initially and then increases slowly, indicating the TUFs can be applied in the protection of cultural relics with various weights. Even at 0.01 kg, the TUFs can still generate a voltage of 0.5 V. In short, with PDMS acting as the triboelectric layer, the TUFs not only has good concealment but also shows great pressure and area sensitivity, which guarantees a promising application for the protection of different sizes of cultural relics.

As for protecting cultural relics from theft, the TUFs is required to respond effectively to cultural relics of different materials for real-time monitoring. Classified by materials, cultural relics can be divided into bronze, iron, gold, silver, porcelain, paintings, calligraphy, handicrafts, etc. Based on this classification, we selected six kinds of materials: rice paper, wood, iron, porcelain, copper, and silk (Fig. 3(a)). They were fabricated into 3 cm \times 3 cm size samples. Then measurements were conducted to investigate how the TUFs responds to these six materials. In addition, the manner may vary when a criminal steals a cultural relic away. Hence no matter how a criminal picks up an artifact from a TUFs, the TUFs should respond effectively. The separation of the artifact

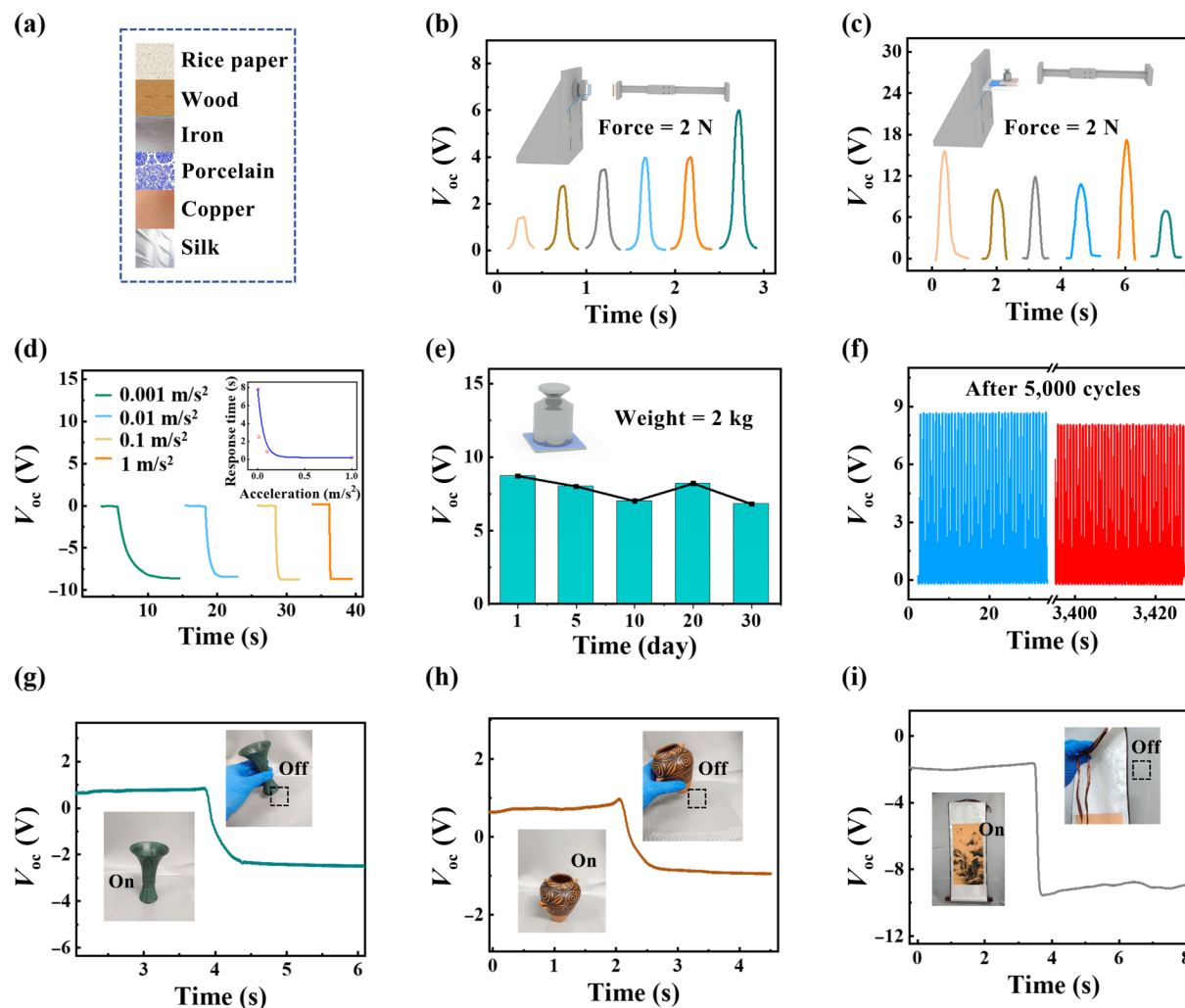


Figure 3 Voltage responses to different cultural-relic materials and stability of the TUFs. (a) Schematics of six cultural-relic materials. (b) and (c) V_{OC} to six cultural-relic materials at (b) the contact-separation mode and (c) the sliding-separation mode (2 N). The insets show the measuring scenes. (d) V_{OC} of different separation accelerations (5 N). (e) V_{OC} at different dwell time. The inset shows the measuring scene. (f) V_{OC} corresponding with continuous operation for 5,000 cycles (5 N). (g)–(i) V_{OC} for (g) a wine bronze cup, (h) a pottery bottle, and (i) a Chinese landscape painting. The insets show the measuring scene. In the black rectangular dashed boxes are TUFs.

from the TUFs can be by contact separation, sliding separation, or a combination of both. Consequently, we constructed two measuring environments to corroborate the performance of the TUFs. A linear motor and a force sensor were used to control the separation manners and force between the sample and the TUFs as shown in the insets of Figs. 3(b) and 3(c).

The orders of six materials from the left to the right (Figs. 3(b) and 3(c)) correspond to the order of six materials from the top to the bottom in Fig. 3(a). Extracting from Figs. 3(b) and 3(c), it is observed that distinct output voltages are produced when these samples are off the TUFs, which is resulted from the high electron gaining capability of PDMS compared with these six materials, verifying the TUFs can respond to a wide range of cultural relics.

Moreover, given that criminals may pick up cultural relics rapidly or slowly, it should be surveyed how the separation velocity influences the V_{OC} . The V_{OC} of the TUFs was measured at 0.001, 0.01, 0.1, and 1 m/s² (Fig. 3(d)). And the $d(V_{OC})/dt$ versus time curves were obtained as depicted in Fig. S2 in the ESM. The response time is defined as the time it takes for $d(V_{OC})/dt$ to increase from zero, decrease and then go to zero. As we can see, there is little change in voltage magnitude whereas the response time decreases as separation speed increases. The inset of Fig. 3(d) shows the relationship between the response time and separation accelerations in which the red solid circle represents the experimental data and the black curve is the fitting curve. Apparently, the separation acceleration affects the response time, but has little influence on the voltage magnitude. Moreover, in museums where objects may not be moved for days or months after they have been positioned, we need to simulate this situation to see if the TUFs will still work. We pressed a 0.5 kg weight onto a 3 cm × 3 cm TUFs, picked it up at different dwell time, and tested the output of the TUFs. As described in Fig. 3(e), the V_{oc} lessens a little with the time prolonging, which is because the charges on the PDMS film dissipate a little. However, it does not affect the function of the TUFs. Because the polymer material is insulated, the dissipation rate of charges on its surface is very slow. Consequently, the amplitude reduction of the V_{oc} is very small with the time prolonging. The V_{oc} is adequate to ensure that the TUFs responds effectively to cultural relics. In other cases, cultural relics may need to be changed or adjusted to their locations, so it is necessary to test the dynamic stability of the TUFs. As shown in Fig. 3(f), a negligible voltage drop is observed after testing for 5,000 cycles, exhibiting good stability of the TUFs. To examine if

the TUFs can respond effectively to practical cultural relics, a TUFs was attached to an acrylic plate with double-sided adhesive, and the V_{oc} was tested for a wine bronze cup and a pottery bottle. The weight of the wine bronze cup and the pottery bottle is illustrated in Figs. S3(a) and S3(b) in the ESM. As shown in Figs. 3(g) and 3(h), the voltage rapidly increases after the wine bronze cup is removed, as does the pottery bottle. Admittedly, the TUFs is hard to be noticed from the corresponding insets owing to its good concealment. Furthermore, a TUFs was affixed to a curtain on which hung a Chinese landscape painting. With the painting off the TUFs, there is a sudden increase of the V_{OC} (Fig. 3(i)). These exceptional output performances substantiate that the TUFs can be employed for the anti-theft of different types of cultural relics.

2.3 Application of the TUFs

We constructed a cultural-relic anti-theft system for realizing the real-time alarming and accurate positioning, which is clarified in Fig. 4(a). First, we fabricated a 2 × 2 TUFs array (Fig. S4 in the ESM), on which placed a three-legged bronze wine cup, a porcelain vase, a bronze mirror, and a jade pendant. Apparently, the TUFs array has a good concealment. The weights of these cultural relics are shown in Figs. S3(c)–S3(f) in the ESM. Then the voltage signal is transmitted into a PC via an acquisition card. Through a program based on the LabVIEW software, the voltage signal is processed and then the program judges whether a cultural relic has been stolen. If the judging results are true, the system will sound an alarm and determine the position of the stolen cultural relic. We simulated intrusion scenarios of the cultural-relic anti-theft system. As exhibited in Fig. 4(b), once the bronze wine vessel is stolen, the system will immediately sound an alarm and the display control of cultural relic 1 turns from grey into red. Same, the system can sound an alarm and position the stolen artifacts successfully when the porcelain vase and the jade pendant are stolen as indicated in Fig. 4(c). The display video of the cultural-relics anti-theft system is shown in Movie ESM1, corroborating the system can be applied in history museums, field artifacts excavation sites, and temporary exhibition events.

3 Conclusions

A transparent, ultrathin, and flexible triboelectric sensor was obtained through coating PDMS uniformly on an ITO-PET

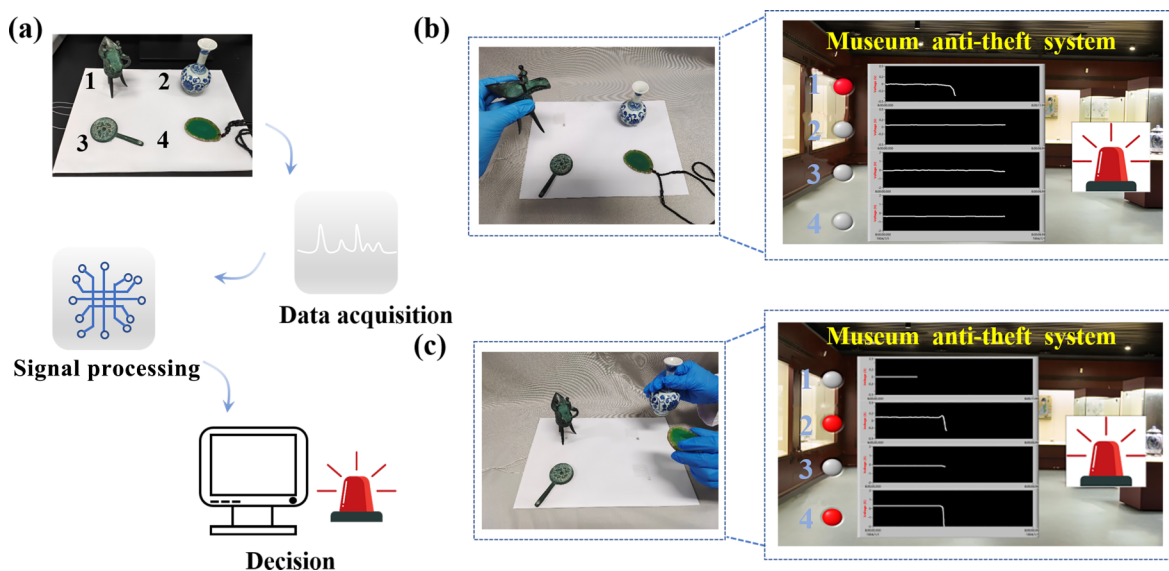


Figure 4 Cultural-relic anti-theft system. (a) Working process of the cultural-relic anti-theft system. (b) Cultural relic 1 is stolen with the corresponding LabVIEW front panel interface. (c) Cultural relic 2 and 4 stolen with the corresponding LabVIEW front panel interface.

substrate. Through rationally selecting materials and adjusting parameters of the spin coating, its thickness, weight, and transmittance are 92 μm , 0.12 g, and 89.4%, respectively, which endows the TUFs with superb concealment. The water contact angle of the TUFs is 106.57°, rendering the TUFs good hydrophobicity. Moreover, a voltage of 0.5 V is observed when the weight is only 10 g and a voltage of 1.5 V is observed when the contact area is 1 cm \times 1 cm, substantiating the TUFs can respond effectively even the artifacts are small and light. Besides, the TUFs responds effectively toward rice paper, wood, iron, porcelain, copper, and silk no matter how cultural relics separate from the TUFs. With separation acceleration rises, the V_{OC} keeps at 10 V generally, indicating the amplitude of V_{OC} is not influenced by the separation acceleration. Furthermore, the TUFs exhibits superior dynamic and static stability. The TUFs is demonstrated to be used effectively for a wine bronze cup, a pottery bottle, and a Chinese landscape painting. Moreover, the triboelectric effect is widely existing in materials, thus the TUFs is expected to applied to a wide range of cultural relics. Finally, a concealed cultural-relic anti-theft system is corroborated to realize real-time alarming and accurate positioning of cultural relics.

4 Experimental section

4.1 Fabrication of the EC-based sensor

2 g EC particles were dissolved in 14 mL anhydrous ethanol to form a 12.5 wt.% clear solution. Then the solution was spin-coated on a 50 μm -thick ITO-PET substrate, which were cured at 80 °C in a vacuum oven for 2 h. Finally, a transparent EC-based sensor was obtained.

4.2 Fabrication of the TUFs

The PDMS elastomer and the curing agent (Sylgard 184, Dow Corning) were thoroughly mixed in the weight ratio of 6:1 with a mechanical blender for 15 min. Then the mixed solution was degassed by vacuum for 30 min and spin-coated uniformly on an ITO-PET substrate with a thickness of 50 μm , followed by curing at 80 °C for 2 h in an oven. A thin copper wire was attached to the ITO electrode to form a complete TENG device. The effective contact area of the device was 3 cm \times 3 cm. The thickness and weight of the sensor were 92 μm and 0.12 g, respectively.

4.3 Characterization and measurements

A linear motor (LinMot BF01-37) was applied to provide the periodic contact-separation movement for TENGs. A programmable electrometer (Keithley, model 6514) was adopted to test the V_{OC} , Q_{SC} , and I_{SC} . The data was transmitted to a PC through an acquisition card (NI BNC-2110) and processed by LabVIEW.

Acknowledgments

This research was supported by the National Natural Science Foundation of China (No. 61503051).

Electronic Supplementary Material: Supplementary material (Fig. S1 shows the weight of the TUFs; Fig. S2 illustrates the relationship between $d(V_{OC})/dt$ and time at acceleration of 0.001 m/s^2 ; Fig. S3 shows the weight of samples for cultural relics; Fig. S4 presents the photograph of the 2 \times 2 sensor array; Movie ESM1 is a demonstration of the concealed cultural-relic anti-theft system) is available in the online version of this article at <https://doi.org/10.1007/s12274-022-4443-y>.

References

- Wei, Q. W.; Yang, C. P. The design of indoor infrared alarm. *Appl. Mech. Mater.* **2014**, *651–653*, 1105–1108.
- Ke, G.; Jiang, Q. J. Application of internet of things technology in the construction of wisdom museum. *Concurr. Comput. Pract. Exp.* **2019**, *31*, e4680.
- Han, J. H.; Ma, Y.; Huang, J.; Mei, X. G.; Ma, J. Y. An infrared small target detecting algorithm based on human visual system. *IEEE Geosci. Remote Sens. Lett.* **2016**, *13*, 452–456.
- Liu, Z. L.; Wang, M.; Qi, S. K.; Yang, C. C. Study on the anti-theft technology of museum cultural relics based on internet of things. *IEEE Access* **2019**, *7*, 111387–111395.
- Chen, S.; Song, Y. J.; Xu, F. Flexible and highly sensitive resistive pressure sensor based on carbonized crepe paper with corrugated structure. *ACS Appl. Mater. Interfaces* **2018**, *10*, 34646–34654.
- Yang, Y.; Pan, H.; Xie, G. Z.; Jiang, Y. D.; Chen, C. X.; Su, Y. J.; Wang, Y.; Tai, H. L. Flexible piezoelectric pressure sensor based on polydopamine-modified BaTiO₃/PVDF composite film for human motion monitoring. *Sens. Actuators A Phys.* **2020**, *301*, 111789.
- Kim, H. J.; Kim, Y. J. High performance flexible piezoelectric pressure sensor based on CNTs-doped 0–3 ceramic-epoxy nanocomposites. *Mater. Des.* **2018**, *151*, 133–140.
- Mishra, R. B.; El-Atab, N.; Hussain, A. M.; Hussain, M. M. Recent progress on flexible capacitive pressure sensors: From design and materials to applications. *Adv. Mater. Technol.* **2021**, *6*, 2001023.
- Fan, F. R.; Tian, Z. Q.; Wang, Z. L. Flexible triboelectric generator. *Nano Energy* **2012**, *1*, 328–334.
- Wang, Z. L. From contact-electrification to triboelectric nanogenerators. *Rep. Prog. Phys.* **2021**, *84*, 096502.
- Wang, Z. L. On the expanded maxwell's equations for moving charged media system—general theory, mathematical solutions and applications in TENG. *Mater. Today* **2022**, *52*, 348–363.
- Rodrigues, C.; Nunes, D.; Clemente, D.; Mathias, N.; Correia, J. M.; Rosa-Santos, P.; Taveira-Pinto, F.; Morais, T.; Pereira, A.; Ventura, J. Emerging triboelectric nanogenerators for ocean wave energy harvesting: State of the art and future perspectives. *Energy Environ. Sci.* **2020**, *13*, 2657–2683.
- Wang, Z. L. Triboelectric nanogenerator (TENG)-sparking an energy and sensor revolution. *Adv. Energy Mater.* **2020**, *10*, 2000137.
- Wu, Z. Y.; Cheng, T. H.; Wang, Z. L. Self-powered sensors and systems based on nanogenerators. *Sensors* **2020**, *20*, 2925.
- Chen, J. H.; Wei, X. L.; Wang, B. C.; Li, R. N.; Sun, Y. G.; Peng, Y. T.; Wu, Z. Y.; Wang, P.; Wang, Z. L. Design optimization of soft-contact freestanding rotary triboelectric nanogenerator for high-output performance. *Adv. Energy Mater.* **2021**, *11*, 2102106.
- Chen, Y. F.; Gao, Z. Q.; Zhang, F. J.; Wen, Z.; Sun, X. H. Recent progress in self-powered multifunctional e-skin for advanced applications. *Exploration* **2022**, *2*, 20210112.
- Zhang, T. T.; Wen, Z.; Liu, Y. N.; Zhang, Z. Y.; Xie, Y. L.; Sun, X. H. Hybridized nanogenerators for multifunctional self-powered sensing: Principles, prototypes, and perspectives. *iScience* **2020**, *23*, 101813.
- Wu, Z. Y.; Guo, H. Y.; Ding, W. B.; Wang, Y. C.; Zhang, L.; Wang, Z. L. A Hybridized triboelectric–electromagnetic water wave energy harvester based on a magnetic sphere. *ACS Nano* **2019**, *13*, 2349–2356.
- Wu, Z. Y.; Zhang, B. B.; Zou, H. Y.; Lin, Z. M.; Liu, G. L.; Wang, Z. L. Multifunctional sensor based on translational - rotary triboelectric nanogenerator. *Adv. Energy Mater.* **2019**, *9*, 1901124.
- Li, R. N.; Wei, X. L.; Xu, J. H.; Chen, J. H.; Li, B.; Wu, Z. Y.; Wang, Z. L. Smart wearable sensors based on triboelectric nanogenerator for personal healthcare monitoring. *Micromachines* **2021**, *12*, 352.
- Wei, X. L.; Zhao, Z. H.; Zhang, C. G.; Yuan, W.; Wu, Z. Y.; Wang, J.; Wang, Z. L. All-weather droplet-based triboelectric nanogenerator for wave energy harvesting. *ACS Nano* **2021**, *15*, 13200–13208.
- Wang, H. Y.; Wang, J. Q.; Yao, K. M.; Fu, J. J.; Xia, X.; Zhang, R. R.; Li, J. Y.; Xu, G. Q.; Wang, L. Y.; Yang, J. C. et al. A paradigm shift fully self-powered long-distance wireless sensing solution

- enabled by discharge-induced displacement current. *Sci. Adv.* **2021**, *7*, eabi6751.
- [23] Wu, H.; Wang, S.; Wang, Z. K.; Zi, Y. L. Achieving ultrahigh instantaneous power density of 10 MW/m² by leveraging the opposite-charge-enhanced transistor-like triboelectric nanogenerator (OCT-TENG). *Nat. Commun.* **2021**, *12*, 5470.
- [24] He, X. M.; Guo, H. Y.; Yue, X. L.; Gao, J.; Xi, Y.; Hu, C. G. Improving energy conversion efficiency for triboelectric nanogenerator with capacitor structure by maximizing surface charge density. *Nanoscale* **2015**, *7*, 1896–1903.
- [25] Guo, H. Y.; Chen, J.; Wang, L. F.; Wang, A. C.; Li, Y. F.; An, C. H.; He, J. H.; Hu, C. G.; Hsiao, V. K. S.; Wang, Z. L. A highly efficient triboelectric negative air ion generator. *Nat. Sustain.* **2021**, *4*, 147–153.
- [26] Meng, K. Y.; Wu, Y. F.; He, Q.; Zhou, Z. H.; Wang, X.; Zhang, G. Q.; Fan, W. J.; Liu, J.; Yang, J. Ultrasensitive fingertip-contacted pressure sensors to enable continuous measurement of epidermal pulse waves on ubiquitous object surfaces. *ACS Appl. Mater. Interfaces* **2019**, *11*, 46399–46407.
- [27] Shi, Q. F.; Zhang, Z. X.; He, T. Y. Y.; Sun, Z. D.; Wang, B. J.; Feng, Y. Q.; Shan, X. C.; Salam, B.; Lee, C. Deep learning enabled smart mats as a scalable floor monitoring system. *Nat. Commun.* **2020**, *11*, 4609.
- [28] Wen, F.; Sun, Z. D.; He, T. Y. Y.; Shi, Q. F.; Zhu, M. L.; Zhang, Z. X.; Li, L. H.; Zhang, T.; Lee, C. Machine learning glove using self-powered conductive superhydrophobic triboelectric textile for gesture recognition in VR/AR applications. *Adv. Sci.* **2020**, *7*, 2000261.
- [29] Yang, X. Y.; Liu, G. Q.; Guo, Q. Y.; Wen, H. Y.; Huang, R. Y.; Meng, X. H.; Duan, J. L.; Tang, Q. W. Triboelectric sensor array for internet of things based smart traffic monitoring and management system. *Nano Energy* **2022**, *92*, 106757.
- [30] Gao, Y. Y.; Liu, G. X.; Bu, T. Z.; Liu, Y. Y.; Qi, Y. C.; Xie, Y. T.; Xu, S. H.; Deng, W. L.; Yang, W. Q.; Zhang, C. MXene based mechanically and electrically enhanced film for triboelectric nanogenerator. *Nano Res.* **2021**, *14*, 4833–4840.
- [31] Liu, L.; Tang, W.; Deng, C. R.; Chen, B. D.; Han, K.; Zhong, W.; Wang, Z. L. Self-powered versatile shoes based on hybrid nanogenerators. *Nano Res.* **2018**, *11*, 3972–3978.
- [32] Lei, H.; Chen, Y. F.; Gao, Z. Q.; Wen, Z.; Sun, X. H. Advances in self-powered triboelectric pressure sensors. *J. Mater. Chem. A* **2021**, *9*, 20100–20130.
- [33] Chen, C.; Wen, Z.; Shi, J. H.; Jian, X. H.; Li, P. Y.; Yeow, J. T. W.; Sun, X. H. Micro triboelectric ultrasonic device for acoustic energy transfer and signal communication. *Nat. Commun.* **2020**, *11*, 4143.
- [34] Ke, K. H.; Chung, C. K. High-performance Al/PDMS TENG with novel complex morphology of two-height microneedles array for high-sensitivity force-sensor and self-powered application. *Small* **2020**, *16*, 2001209.
- [35] Shi, Y. P.; Wei, X. L.; Wang, K. M.; He, D. D.; Yuan, Z. H.; Xu, J. H.; Wu, Z. Y.; Wang, Z. L. Integrated all-fiber electronic skin toward self-powered sensing sports systems. *ACS Appl. Mater. Interfaces* **2021**, *13*, 50329–50337.
- [36] Sun, J.; Zhou, W. H.; Yang, H. B.; Zhen, X.; Ma, L. F.; Williams, D.; Sun, X. D.; Lang, M. F. Highly transparent and flexible circuits through patterning silver nanowires into microfluidic channels. *Chem. Commun.* **2018**, *54*, 4923–4926.
- [37] Zou, H. Y.; Zhang, Y.; Guo, L. T.; Wang, P. H.; He, X.; Dai, G. Z.; Zheng, H. W.; Chen, C. Y.; Wang, A. C.; Xu, C. et al. Quantifying the triboelectric series. *Nat. Commun.* **2019**, *10*, 1427.